Cold-Rydberg-gas dynamics

A. Walz-Flannigan, J. R. Guest, J.-H. Choi, and G. Raithel*
FOCUS Center, University of Michigan, Ann Arbor, Michigan 48109-1120, USA
(Received 13 August 2003; revised manuscript received 24 March 2004; published 7 June 2004)

Using state-selective field ionization, the state distributions of Rydberg atoms in cold Rydberg gases are measured for various initially excited Rydberg levels, populations, and evolution times. We provide direct experimental evidence for *l*-changing collisions that we previously observed indirectly [S. K. Dutta, D. Feldbaum, A. Walz-Flannigan, J. R. Guest, and G. Raithel, Phys. Rev. Lett. **86**, 3993 (2001)]. We also observe *n*-mixing and find that its effects are largely in agreement with recent theoretical work on *n*-changing collisions between electrons and Rydberg atoms, thus enabling an estimation of the electron temperature. Unexpectedly large populations of atoms are found in states with principal quantum numbers much lower than that of the initially excited atoms. We explain this observation by collisions between high-*l* Rydberg atoms, which are highly polar and can collide due to static electric-dipole forces between them.

DOI: 10.1103/PhysRevA.69.063405 PACS number(s): 32.80.Pj, 32.80.Rm, 52.25.Ya

I. INTRODUCTION

Gases of cold Rydberg atoms and plasmas produced by laser excitation of clouds of cold atoms prepared in magneto-optic traps (MOTs) have been the subject of numerous recent studies. These systems provide a collision-rich environment which has revealed the spontaneous transformation of a cold Rydberg gas to a plasma [1,2], Rydberg atom formation from three-body recombination in an ultracold plasma [3], and *l* mixing due to interactions between electrons and cold Rydberg atoms [4]. The expansion dynamics of ultracold plasmas has been addressed in theoretical [5–7] and experimental [8] work. There remain outstanding questions regarding the evolution of cold-Rydberg-atom gases. To what degree is the initially excited state depleted? To what degree is the final-state distribution the result of *l*-mixing, inelastic collisions, Rydberg-Rydberg collisions, thermal redistribution or three-body recombination? How exactly are the final states distributed over *n* and *l*?

In this paper, we show that in gases of cold Rydberg atoms the regimes of *l*-mixing, *n*-mixing, and collision-induced ionization are clearly correlated with experimental parameters (number of atoms, evolution time, and initial Rydberg state). In addition to confirming earlier indirect observations of *l*-mixing [4], our data provide experimental evidence for inelastic *n*-mixing collisions between electrons and Rydberg atoms which have been predicted to be significant in cold Rydberg gases [5]. In agreement with Ref. [5], we observe *n* mixing mostly into states with principal quantum numbers higher than that of the initially excited Rydberg state. Unexpectedly, we also find large populations of Rydberg atoms in states with very low *n*, indicating large collisions rates between cold Rydberg atoms and other cold Rydberg atoms (as opposed to room-temperature Rydberg atoms [2]). We believe that the Rydberg-Rydberg collisions are triggered by interatomic forces between highly polar high-*l* Rydberg atoms, which are generated through *l*-mixing collisions.

*graithel@umich.edu; URL: http://quaser.physics.lsa.umich.edu

II. SUMMARY OF PROCESSES IN A COLD RYDBERG GAS

The way in which a cold Rydberg gas evolves is strongly influenced by the conditional formation of an electron trap [1], which is briefly reviewed in the following. During and shortly after the excitation of a cold Rydberg gas, a small fraction of the Rydberg population ionizes. In our system, this may result from the direct ionization of atoms by amplified spontaneous emission (ASE) in our Rydberg-excitation laser and from partial thermal ionization of the Rydberg atoms. As electrons leave the gas, the remaining ions create a positive space charge, forming a potential well for subsequent free electrons. The depth of the potential seen by a *single* electron left in a Gaussian ion cloud equals $\sqrt{2/\pi}(N_i e/(4\pi\varepsilon_o\sigma))$ (in eV), where N_i is the ion number and σ the rms radius of the ion cloud. When the depth exceeds the kinetic energy of the free electrons, a fraction of the electrons are trapped. The resulting ultracold plasma and the associated electron trap dissipate over tens of μs [1]. During the dissipation time, the trapped-electron cloud and the remainder of the original Rydberg-atom cloud coexist and interact.

The presence of the plasma electron trap is critical for electron-Rydberg atom collisions. Without the electron trap, electrons would pass through the atom cloud only once and escape on nanosecond time scales. For trapped electrons, the interaction time $t_{\rm int}$ between an electron and the Rydberg gas can increase over 1000 fold. This greatly increases the probabilities P of all collisional processes between Rydberg atoms and electrons,

$$P = Rt_{\rm int}, \tag{1}$$

with R denoting the collision rates of the possible types of electron-Rydberg collisions.

The relevant electron-Rydberg collisions can be classified as (nearly) elastic *l*-changing, inelastic *n*-changing, and ionizing. At the extreme of large Rydberg-atom populations the electron density becomes sufficiently large that most of the Rydberg gas is ionized. At densities low enough that ioniza-

 ©2004 The American Physical Society

tion does not dominate, or at times before ionization processes in the gas have saturated, the effect of nonionizing collisions between electrons and Rydberg atoms can be observed. The window in which we can observe these nonionizing collisions can be described by the requirement that

$$P_{\mathrm{coll}} \lesssim 1 \text{ and } P_{\mathrm{ion}} \ll 1, \tag{2}$$

i.e., the probability P_{coll} of nonionizing collisions is significant yet the probablility P_{ion} of ionizing collisions is small. This window depends on the type of nonionizing collision, the trapped-electron temperature and density, the interaction time t_{int}, and the initial Rydberg state (in a manner reflecting the n dependence of the collision cross sections). Nonionizing collisions between electrons and Rydberg atoms are investigated in detail in Secs. V B and V C.

There are other relevant types of collisions in a cold Rydberg gas. We find a very large population of Rydberg atoms in states with principal quantum numbers much smaller than that of the initial state. Since inelastic collisions between Rydberg atoms and charged particles typically favor transitions into neighboring n levels (as do charge-exchange collisions between Rydberg atoms and ions) [9], there must be another important type of collision process. We believe that the appearance of low-n states is a result of collisions between cold Rydberg atoms (see discussion in Sec. V D). In addition, three-body recombination [3] may play a minor role in explaining the data shown in this paper. However, our electron densities are too small for it to be a dominant or clearly discernible process.

III. EXPERIMENTAL METHOD

Our cold Rydberg gas is formed by exciting ^{85}Rb atoms with temperatures $\approx 100\ \mu$K in a UHV (ultrahigh vacuum) MOT, which is loaded with a cold, slow beam of atoms emitted from a low-velocity-intense-source (LVIS) [10], as detailed in Fig. 1. An auxiliary magnetic-field coil is placed near the LVIS such that the location of zero magnetic field, and hence the trap center, can be shifted in and out of the LVIS extraction column. This allows us to control the atom flux from the LVIS to the UHV MOT and therefore the UHV MOT population. The UHV MOT provides an environment in which the background pressure of room-temperature Rb vapor is negligible. This allows us to rule out collisions between slow Rydberg atoms and hot ones excited from room-temperature Rb vapor, as reported in Ref. [2].

The experiment is run on a ~ 1 Hz cycle, with a continuous flux of slow atoms (≈ 10 m/s) from the LVIS to the UHV MOT. The Rydberg states are populated using two-step excitation. The first transition, from the $5S_{1/2}$, $F=3$ to the $5P_{3/2}$, $F=4$ manifold, is excited using the MOT light or a separate, on-resonant laser pulse of $\approx 5\ \mu$s duration ($\lambda \approx 780$ nm). A tunable pulsed dye laser (PDL) ($\lambda \approx 480$ nm), pulse width ≈ 10 ns, bandwidth ≈ 15 GHz) is used to excite the ^{85}Rb atoms into nd- or ns-Rydberg states. The PDL pulses have a typical energy of 100–200 μJ with a fluence of $\Phi \sim 3 \times 10^{15}$ cm^{-2}. The MOT light and magnetic field remain on during the Rydberg excitation.

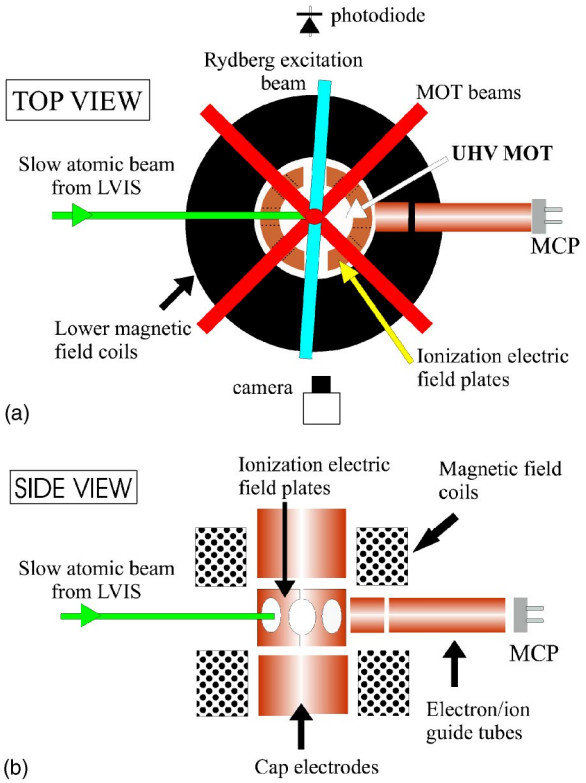

FIG. 1. (a) Top view, in cross section, and (b) side view of the experimental setup.

Rydberg atoms are detected and identified using state-selective field ionization. In our experiments, the ionization electric field has a maximal value of ≈ 220 V/cm at the position of the MOT and is applied using two semicircular electrodes that encircle the MOT. The field-ionization (FI) pulse is applied in an approximately linear ramp with a rise time of 30 μs. Electrons released by field ionization propagate through a set of guide tubes to a microchannel plate detector positioned 12.5 cm from the MOT center. Because in the FI process the multidimensional state space $\{|n,n_1,n_2\rangle\}$ is mapped onto the one-dimensional axis of the ionization electric field, a given ionization electric field does not uniquely identify a single quantum state (n_1 and n_2 denote parabolic quantum numbers) [11]. Therefore, there is some ambiguity in assigning Rydberg states to FI spectra. Nevertheless, as explained in Sec. V, a clear interpretation of most observations can still be obtained.

Demonstration of how and when the different collisional processes occur requires knowledge of the initial Rydberg-atom populations and densities. The total population N_{P} of atoms in the $5P_{3/2}$ state is obtained by fluorescence measurement. The uncertainty of N_{P} is fairly low (about 10%). The physical size of the atom cloud is determined by fitting charge-coupled device images of the MOT with two-dimensional Gaussians, yielding Gaussian widths σ_{2D}. Assuming that the volume density distribution of the atoms in the MOT is described by a three-dimensional (3D) Gaussian having a width σ_{3D} identical to σ_{2D}, we can establish the central volume density of atoms in the $5P_{3/2}$ state, ρ_{P}, by equating the volume integral of the 3D Gaussian to the total

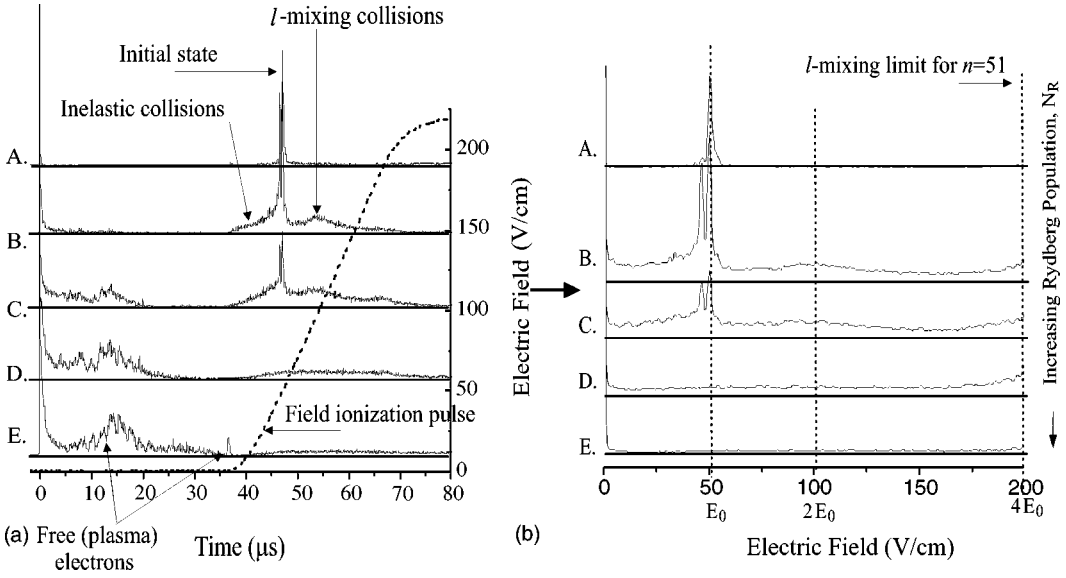

FIG. 2. Field-ionization spectra for initially excited 51*d* states. Panel (a): FI signal and the FI pulse vs time. The FI pulse arrives 38 μs after the Rydberg excitation ($t \approx 0$). The signal prior to the FI pulse is due to escaping plasma electrons. Panel (b): Field-ionization data of panel (a) mapped into a function of ionization electric field. Note that in (b) all signal prior to the application of the FI pulse is condensed into a single peak at 0 V/cm (and therefore is hardly visible). The traces *A*–*E* correspond to the following initial Rydberg-atom populations N_R and densities ρ_R. *A*, N_R and ρ_R very small; *B*, $N_R = 5.5 \times 10^2$ and $\rho_R = 2.7 \times 10^8$ cm^{-3}; *C*, $N_R = 5.4 \times 10^3$ and $\rho_R = 5.9 \times 10^8$ cm^{-3}; *D*, $N_R = 7.0 \times 10^5$ and $\rho_R = 2.2 \times 10^9$ cm^{-3}; *E*: $N_R = 3.3 \times 10^6$ and $\rho_R = 9.6 \times 10^8$ cm^{-3}.

population N_P. Since the MOT volume density profile is neither Gaussian nor spherically symmetric, the uncertainty of the central atom density ρ_P is considerably larger than that of N_P. We expect our ρ_P values to be accurate within a factor of 2.

The fluence Φ of the blue 480 nm laser pulses is measured as follows. A small photodiode with well defined area and quantum efficiency is placed at the center of the blue laser beam at a location equivalent to that of the atom cloud. The blue laser is attenuated by a factor large enough to avoid saturation of the photodiode. Integration of the photo current over the pulse duration then yields the fluence Φ at the center of the blue pulses with an uncertainty of about 10%. Since the blue laser beam has a diameter of $\sim$3 mm, it completely envelopes the cold-atom cloud collected by the MOT. Thus, far from saturation, the Rydberg-atom number N_R is found by $N_R = N_P \Phi \sigma_R$, where σ_R is the photo-excitation cross section for the desired Rydberg state. A similar equation, $\rho_R = \rho_P \Phi \sigma_R$, applies for the central Rydberg-atom density ρ_R.

Since the photoexcitation cross section of Rb *d* states is about six times larger than that of neighboring *s* states, N_R can be determined with sufficient accuracy by considering only excitation into *d*-Rydberg states. For excitation into the *d*-state continuum the photo-excitation cross section is $\sigma_{ion} = 1.2 \times 10^{-17}$ cm^2 [12]. The same cross section applies for excitation into bound states $n_0 d$ with the initial-state principal quantum number n_0 high enough that neighboring levels cannot be resolved, i.e., if the laser linewidth, measured in atomic units, satisfies $\Delta\omega \geq 1/n_0^3$. In our case, this condition is valid for $n_0 \gtrsim 70$. For excitation into lower Rydberg states the cross section is [9]

$$\sigma_R = \frac{\sigma_{ion}}{n_0^3 \Delta\omega} = \frac{1.2 \times 10^{-17}\ \text{cm}^2}{n_0^3 \Delta\omega}. \quad (3)$$

IV. EXPERIMENTAL RESULTS

A. Field-ionization spectra vs initial Rydberg-atom number

We first present the dependence of the evolution of Rydberg gases on the initial Rydberg-atom population, N_R. Figure 2 shows FI spectra for initially excited 51*d* Rydberg states, Fig. 3 for 65*d* states. The original time-dependent data [panels (a)] show the time dependence of the FI electric field and the electron signal obtained prior to and during application of the FI pulse. The FI pulse is applied 38 μs and 18 μs after the Rydberg-atom excitation in Figs. 2 and 3, respectively. In panels (b), the data of panels (a) have been processed in order to show the FI signal vs ionization electric field.

Shown in traces *A* of these figures are the FI spectra of Rydberg states excited from a cold atomic beam. In this case, there is no UHV MOT, and consequently the Rydberg-atom numbers and densities are minimal. Collision processes are therefore largely absent in traces *A*, and the only peaks present in the FI signal are from the respective initially excited states. Traces *A* provide baselines for the extent of thermal redistribution among the Rydberg state population during the time before the FI pulse is applied. In accordance with thermal transition rates for individual Rydberg-Rydberg transitions [9] and rate-equation simulations including large-state spaces [13], thermal redistribution among bound Rydberg levels is not a significant factor in our system. We note that there also is thermal ionization with a typical yield of order 0.01 thermal electrons per atom over 50 μs [13]. The thermal electrons can be important, because they participate in the collisions described in Secs. V B and V C.

If the UHV MOT is turned on, the initial Rydberg-atom population becomes significant. Due to ASE, a fraction of the

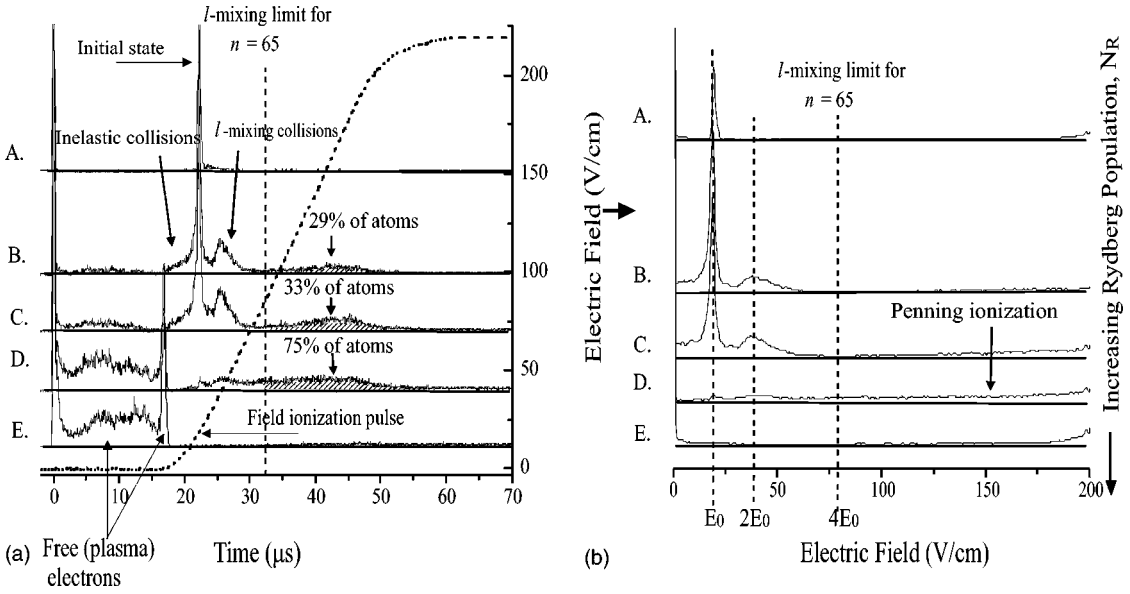

FIG. 3. Field-ionization spectra for initially excited 65*d* states. Panel (a): FI signal and FI pulse vs time. The FI pulse, indicated by the dashed line, arrives 18 μs after the Rydberg excitation ($t \approx 0$). Panel (b): FI data of panel (a) mapped as a function of ionization electric field. In (b), all signal arriving prior to the application of the FI pulse is condensed into a single peak at 0 V/cm (and therefore is hardly visible). The traces $A-E$ correspond to the following initial Rydberg-atom populations N_R and densities ρ_R. *A*, N_R and ρ_R very small; *B*, $N_R = 8.4 \times 10^2$ and $\rho_R = 1.0 \times 10^8$ cm^{-3}; *C*, $N_R = 1.1 \times 10^4$ and $\rho_R = 7.6 \times 10^8$ cm^{-3}; *D*, $N_R = 2.2 \times 10^5$ and $\rho_R = 2.7 \times 10^9$ cm^{-3}; *E*, $N_R = 1.1 \times 10^6$ and $\rho_R = 1.1 \times 10^9$ cm^{-3}. As indicated by the shaded regions, in traces *B*, *C* and *D* at least 29%, 33%, and 75% of the remaining Rydberg atoms have been transferred to lower-*n* states, respectively.

$5P$ atoms are ionized immediately, producing a large, narrow peak immediately following the Rydberg excitation. Additional free electrons are subsequently generated by blackbody thermal ionization and collisions. If a sufficient number of electrons escape within a sufficiently short time, subsequent electrons become temporarily trapped in a cold plasma, as described in Sec. II. During the expansion of the plasma, which occurs over a time period of tens of microseconds, plasma electrons boil off and produce a signal which can be easily observed in the form of a slowly varying electron flux during the external-field-free phase between the excitation and the arrival of the FI pulse. This signature of plasma electrons is seen clearly in the traces $B-E$ of Figs. 2(a) and 3(a), and increases with initial Rydberg population N_R. We find free- (plasma) electron signals even for very small Rydberg populations and trap diameters, shown in trace *B* of both Figs. 2(a) and 3(a). At the time instant when the FI pulse is applied, any remaining trapped plasma electrons are extracted and detected at the very onset of the FI pulse. This is manifested in the spike at $t \approx 38$ μs in trace *E* of Fig. 2(a) and at $t \approx 18$ μs in traces *D* and *E* of Fig. 3(a). The differences between the bound-state FI spectra in traces $A-E$ in Figs. 2 and 3 is largely due to collisions between electrons and Rydberg atoms, described in Sec. V.

B. Field-ionization spectra vs evolution time

An example of the time evolution of a Rydberg gas is shown in Fig. 4 for the case of $n_0 = 64$. There, the evolution time, t_{int}, is controlled independently by varying the delay time between the Rydberg excitation and the FI pulse while holding the initial size and density of the gas constant. When the FI pulse is applied, the free (plasma) electrons are extracted and electron-Rydberg atom collisions cease. Panel (a) in Fig. 4 shows the FI signal as a function of time. The data of panel (a) is processed and shown in panel (b) as a function of ionization electric field.

For the cold Rydberg gas shown in Fig. 4 there is a nearly immediate redistribution of the Rydberg population away from the initial state. This can already be seen at 0.6 μs after excitation (trace *A*). At longer evolution times (traces $B-D$) the FI signal of bound Rydberg states becomes increasingly featureless, reflecting the progressive alteration of Rydberg atoms due to ongoing collision processes. The initial-state features seem to reappear in traces *E* and *F*. Future investigations are required to explain this. Further details of Fig. 4 are discussed in Sec. V.

V. INTERPRETATION OF THE DATA

A. *l* mixing

In previous experiments on cold Rydberg gases, we observed a slowly decaying electron signal that persisted for times on the order of 10 ms after the Rydberg atom excitation. This is orders of magnitudes longer than the lifetime of the initially excited Rydberg states [4]. We argued that the slowly decaying signal could be explained by the formation of Rydberg atoms in high-*l* states with lifetimes on the order of 10 ms, and subsequent partial thermal ionization of these atoms. As explained in the following, the results in Sec. IV of this paper, obtained using state-selective field ionization, confirm the presence of these high-*l* Rydberg atoms. It is also shown in a direct way that these atoms are produced by

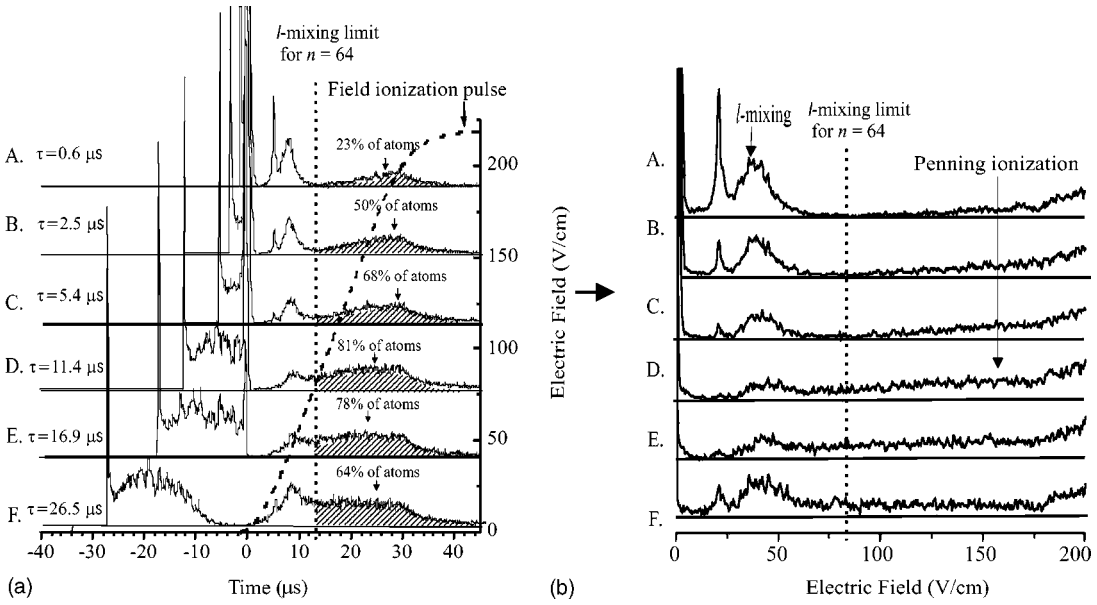

FIG. 4. FI signal from a Rydberg gas with initial state 64*d* shown for the indicated delay times, τ, between the Rydberg excitation and the FI pulse for fixed $N_R = 3.7 \times 10^6$ and $\rho_R = 7.8 \times 10^8$ cm^{-3}. Panel (a): FI signal (solid lines) and FI pulse (dashed line) vs time. The onset of the FI pulse is at $t \approx 0$. Panel (b): data of (a) represented as a function of ionization electric field. In all cases except trace *F*, the delay time τ is equivalent to the interaction time t_{int} between the trapped electrons and the Rydberg-atom gas. The shaded regions in panel (a) indicate the signal from atoms which have been transferred to states with $n \ll n_0$. The percentages of the latter vs the total Rydberg population at the onset of the FI pulse are at least 23%, 50%, 68%, 81%, 78%, 64% for traces *A*–*F*, respectively [3,5].

collisions between Rydberg atoms and electrons.

The ionization electric fields of Rydberg states with initial principal quantum number n_0 and arbitrary parabolic quantum number (n_1 and n_2) are in the range from $E_0 = 1/16n_0^{*4}$ to $4E_0 = 1/4n_0^{*4}$ ([11]; fields in atomic units, n_0^* denotes the effective quantum number of the initial state). In the case of initially excited 51*d* states, shown in Fig. 2, atoms with principal quantum number n_0 and arbitrary n_1 and n_2 have ionization electric fields in the range from $\approx$50 V/cm to $\approx$200 V/cm; the corresponding range in Fig. 3 is $\approx$19.5 V/cm to $\approx$78 V/cm and Fig. 4 is $\approx$21 V/cm to $\approx$84 V/cm. In traces *B* and *C* of Fig. 2, traces *B*–*D* of Fig. 3 and all traces in Fig. 4, a large fraction of the field-ionization signal shifts from the initial peak at the ionization electric field E_0 to a broad peak centered at $\approx 2E_0$. This behavior is typical for *l* mixing [9,14], providing strong evidence that *l* mixing is the physical origin of the FI peaks near $2E_0$. This peak will henceforth be referred to as the "*l*-mixing" peak.

Our interpretation of the *l*-mixing peak is supported by several lines of evidence. The *l*-mixing peak in the FI signal scales with the ionization field E_0 of the initial state and it is absent at very low Rydberg-atom densities (trace *A*, Figs. 2 and 3). Also, as *l*-mixing has the largest of the electron-Rydberg collision cross sections, it is expected to manifest itself first with increasing number of free (plasma) electrons. This agrees with the observed behavior of the *l*-mixing peak.

The conclusion that *l*-mixing collisions between Rydberg atoms and electrons are, under suitable conditions, a dominant process in the system is also supported by numerical estimates of the collision probabilities. The rate R_l of *l*-mixing collisions between slow Rydberg atoms embedded in a plasma with electron density η_e and average electron velocity v_e is

$$R_l = \eta_e \sigma_l(n_0, v_e) v_e, \tag{4}$$

where $\sigma_l(n_0, v_e)$ is the collision cross section for *l*-mixing collisions. The collision rates R_l do not depend on the Rydberg-atom velocities, because the Rydberg atoms are orders of magnitude slower than the electrons. The cross sections $\sigma_l(n_0, v_e)$ depend on the initial Rydberg state n_0 and to a lesser degree on the electron velocity. We have calculated σ_l by numerically integrating the Schrödinger equation over the time of the collision [13]. Using the results for σ_l, Eqs. (1) and (4), we have found that over a 10 μs interaction time less than 1000 trapped electrons can lead to near-unity *l*-mixing probabilities. The calculations have also shown that a single *l*-mixing collision between a Rydberg atom and an electron is sufficient to promote the Rydberg atom into a state with a very large *l* average ($\langle l \rangle \sim n_0/2$). The above estimates have been made for electron temperatures of about 10 meV, in accordance with the bandwidth of the ASE of the utilized blue laser ($\sim$5 nm) and the energy distributions of electrons generated by thermal ionization of Rydberg atoms in a 300 K radiation field (obtained by quantum-mechanical rate-equation simulations [13]).

B. Inelastic collisions

Figures 2–4 show a significant shift in the FI signal to ionization electric fields lower than E_0. This shift is indicative of the redistribution of Rydberg-atom population into states with principal quantum numbers $n > n_0$. For low values of n_0, the redistribution into neighboring *n* levels with

$|n-n_0| \lesssim 2$ can be resolved in our data (see, for instance, curves *B* and *C* in Fig. 2). To our knowledge, this is the first experimental observation of such a redistribution in cold-Rydberg-atom gases. The most likely cause is *n*-changing inelastic collisions between Rydberg atoms and electrons, which have been considered theoretically in Refs. [5,15]. To support this conclusion, in the following we estimate the rates of inelastic collisions between thermal electrons and Rydberg atoms for our parameters.

The total deexcitation rate of a Rydberg atom with energy E_R is given by [5,15]

$$A_d = 7.2\,\eta_e \left(\frac{27.2\ \text{eV}}{k_B T_e}\right)^{0.17} \nu^{2.66} a_0^2 \alpha c, \tag{5}$$

and the total excitation rate, including collisional ionization, is

$$A_e = 55\,\eta_e \left(\frac{k_B T_e}{27.2\ \text{eV}}\right)^{0.83} \nu^{4.66} a_0^2 \alpha c, \tag{6}$$

where η_e is the electron density, k_B Boltzmann's constant, T_e the electron temperature, $\nu = \sqrt{-13.6\ \text{eV}/E_R}$, a_0 the Bohr length, α the fine-structure constant, and c the speed of light. The total inelastic collision rate for each Rydberg atom is

$$R_n = A_d + A_e. \tag{7}$$

The probability of excitation $[A_e/(A_e+A_d)]$ is given by $f = 1/[1-E_R/(3.82 k_B T_e)]$ for atoms experiencing an inelastic collision. For an initially excited $n_0 = 51$ state, an electron energy of $k_B T_e \approx 3$ meV and an electron density of 1×10^6 cm^{-3}, one estimates a total inelastic collision rate per Rydberg atom $R_n \approx 2.1\times10^4$ s^{-1}. For a typical plasma dissipation time of $t_{int} = 30$ μs, Eq. (1) and Eqs. (5)–(7) return a probability $P \approx 0.6$ of the Rydberg atoms experiencing an inelastic collision. A fraction of $f = 68\%$ of the inelastic collisions would cause excitation into higher states or ionization.

In the following, we compare an experimental FI spectrum with calculated outcomes of inelastic collisions between Rydberg atoms and electrons. Since the simulations consider only single collision events, for the comparison we use an experimental result in which the initial Rydberg peak is not severely depleted, i.e., $P_{coll} \ll 1$ [trace *B* of Fig. 2(b); $n_0 = 51$]. In Fig. 5 we compare this experimental FI spectrum with corresponding *n*-mixing simulations for thermal electron energies of 1 meV, 3 meV, and 10 meV.

To obtain the simulated data in Fig. 5, we first follow Ref. [5] to determine the final-state probability distributions $P(n)$ as a function of principal quantum number *n*. Then, $P(n)$ is transformed into a probability distribution of the ionization electric field, $\tilde{P}(E)$. Thereby, we assume that the *n* mixing is not accompanied by significant *l* mixing (i.e., the *n*-mixed atoms are assumed to ionize at an FI electric field of $1/16n^{*4}$). We limit the comparison between the *n*-mixing simulations and the experimental FI spectrum to an electric-field range from 4 V/cm to 42 V/cm, where $42\ \text{V/cm} < E_0 \approx 50\ \text{V/cm}$. The electric-field range $E > E_0$ is excluded from the comparison because of the overlapping effect of *l* mixing. We also exclude the range $42\ \text{V/cm} < E < 50\ \text{V/cm}$, because transitions into states with *n* very close to n_0 are expected to be strongly influenced by the detailed quantum structure of the atom (quantum defects, etc.), which is not modeled in the calculation (which is based on classical mechanics). The range $E < 4$ V/cm is excluded because in that range the experimental data could be complicated by plasma electrons and possibly by three-body recombination.

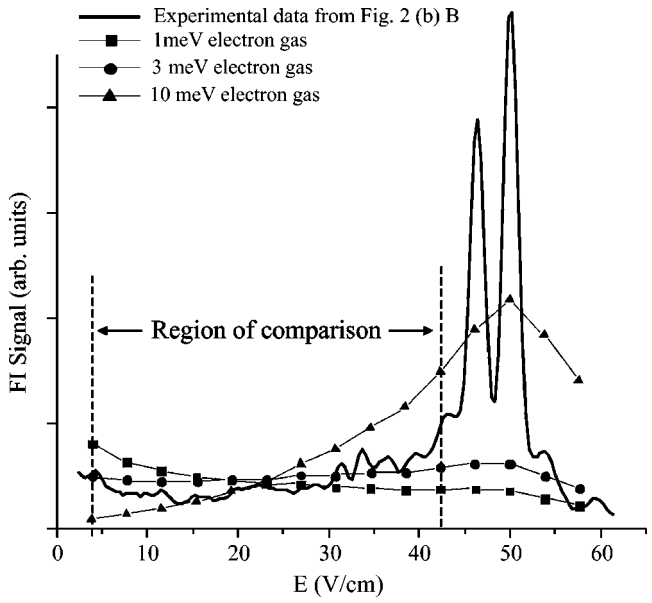

FIG. 5. Simulations of FI signals due to inelastic collisions between electrons and 51*d* Rydberg atoms, compared with the experimental data in trace *B* in Fig. 2(a). Simulations for three different electron energies are shown: $k_B T_e = 1$ meV, 3 meV, and 10 meV. Each simulation result is scaled such that its integral equals that of the experimental result over the region of comparison.

As seen in Fig. 5, in the range of comparison the simulated FI signal for $k_B T_e = 3$ meV and the experimental data are in qualitative agreement, while the simulated FI signals for $k_B T_e = 1$ meV and $k_B T_e = 10$ meV clearly diverge from the experimental data. We conclude that it is very likely that *n*-changing electron-Rydberg atom collisions cause most of the experimentally observed population redistribution into states with ionization fields $E < E_0$, and that for the conditions of Fig. 5 the average thermal electron energy is on the order of 3 meV. The fitting method presented in Fig. 5 can serve as a tool to estimate the electron temperature.

An open question remains as to how much *n*-mixing collisions are coincident with *l* mixing (or not). Our experimental evidence suggests that *n*-mixing collisions mostly leave these atoms in low-*l* (nonhydrogenic) states. If the collisions populating these higher *n* states also changed *l* significantly, we would expect the corresponding signal to be spread between E_n (the ionization electric field for principal quantum number *n* and $l \lesssim 2$) and $4E_n$. This is further evidenced in data where the initially excited state is of lower *n* ($n_0 \lesssim 50$). In such cases we were able to resolve transitions into a succession of states with $n > n_0$, as shown in Fig. 6 for $n_0 = 38$.

C. Evidence of Penning ionization

The data shown in Figs. 2–4 include indications of another inelastic process. As is manifested in these figures,

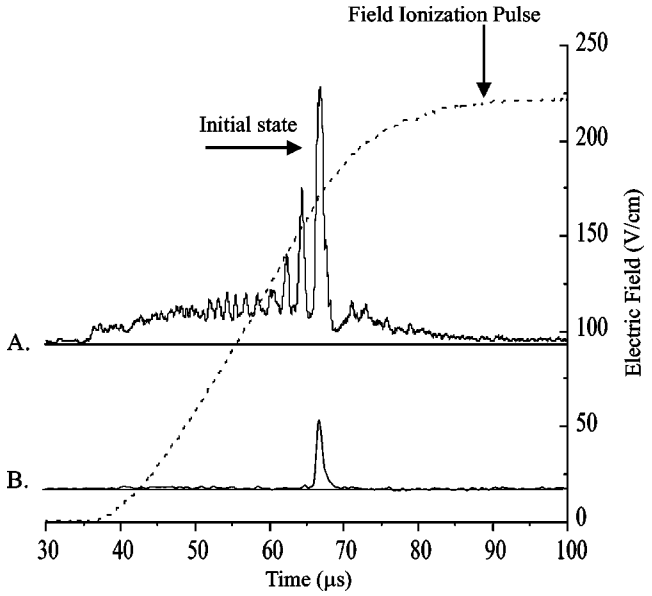

FIG. 6. Field-ionization spectra for initially excited 38*d* states, clearly showing population redistribution to several resolved higher-*n* states. The FI pulse, indicated by the dashed line, starts at 35 μs after the Rydberg excitation. Trace *A*: Initial Rydberg atom population $N_R = 1.1 \times 10^6$ and density $\rho_R = 1.0 \times 10^9$ cm^{-3}. Trace *B*: Reference signal obtained with very small N_R and ρ_R.

there is a significant population shift to ionization electric fields higher than $4E_0$, i.e., beyond the range of *l* mixing of the initial state. Thus, this signal cannot be the result of *l*-mixing collisions alone; it must be due to a process that produces Rydberg states with principal quantum numbers significantly lower than that of the initial state. The shift of Rydberg population into states with $n \ll n_0$ is especially prominent in Fig. 3, traces *B*–*D*, where at least 29%, 33%, and 75% of the remaining Rydberg atoms are in states with $n \ll n_0$, and again in Fig. 4, traces *A*–*F*, where up to 81% of the remaining Rydberg atoms are in states with $n \ll n_0$. In Figs. 2–4, it is also clear that some of the Rydberg population in states with $n \ll n_0$ is not detected because of the voltage limitation of the FI pulse.

In general, the percentage of the population shift into states with $n \ll n_0$ can become very large, and it appears to increase with initial Rydberg atom number, as seen in Fig. 3. Figure 4 further suggests that the shift into states with $n \ll n_0$ may saturate and sometimes moderately decrease with interaction time. The decrease in traces *E* and *F* of Fig. 4 could have been an isolated experimental artifact or a result of processes adding population into higher-*n* states such as three-body recombination [3].

While inelastic collisions discussed in the preceding section can result in some Rydberg atoms with $n < n_0$, the experimentally observed high percentages of atoms in such states and the increase of population with decreasing *n* observed in the range of very low *n*, are in strong contradiction with the behavior one would expect for inelastic electron-Rydberg-atom collisions [5,15]. Thus, inelastic electron-Rydberg-atom collisions cannot explain the experimentally observed quantity of Rydberg atoms in states $n \ll n_0$. This leads us to believe that those atoms are the product of Penning ionization of cold-Rydberg-atom pairs.

Penning ionization has been previously observed between cold and room temperature (and therefore fast) Rydberg atoms [2]. In our UHV system, the number of room-temperature Rydberg atoms is negligible. Because all of the Rydberg atoms in our system are initially cold (with velocities $\sim$10 cm/s), a significant rate of Rydberg-Rydberg collisions would only be facilitated by attractive forces between the Rydberg atoms. In atomic-beam experiments [16], interatomic forces have been observed to lead to enhanced rates for Penning ionization between Rydberg atoms of one species and ground-state atoms of another. In our experiment, very strong attractive forces can occur between cold Rydberg atoms with permanent dipole moments. As discussed above, *l* mixing transfers a significant fraction of the initial population to higher-*l* states. While the initial states have permanent dipole moments near zero, the average *l*-mixed state will have a dipole moment that scales as ea_0n^2. The dipoles of the *l*-mixed atoms are randomly oriented. Two atoms that happen to experience a mutual attractive force are accelerated towards one another, allowing them to collide.

For *l*-mixed $n_0 = 65$ Rydberg atoms in a gas of density $\rho_R = 10^8$ cm^{-3} we have estimated that attractive dipole forces can cause Rydberg atoms starting at the average nearest-neighbor separation to snap together in $\approx$10 μs. For higher densities, $\rho_R = 10^9$ cm^{-3}, this average "snap" time is $\approx$2 μs. Based on these estimates, both in Figs. 3 and 4 we expect to observe the effects of collisions between high-*l* Rydberg atoms. Under the conditions of Fig. 4 ($n_0 = 65$, high Rydberg-atom density) it is not unreasonable to expect such effects even for the shortest interaction time between electrons and Rydberg atoms ($t_{int} = 0.6$ μs). At that time there is already a significant population in high-*l* Rydberg states, which may still collide during the first several μs of the FI pulse.

Among the outcomes of Rydberg-Rydberg atom collisions, Penning ionization

$$\mathrm{Rb}^{**} + \mathrm{Rb}^{**} \rightarrow \mathrm{Rb}^{+} + \mathrm{Rb}^{*} + e^{-}, \tag{8}$$

is expected to be the most prevalent [17]. In this collisional process, the ionization energy of one atom is taken from the deexcitation of its collision partner to a lower-*n* state. Based on the described evidence, we believe that the observed Rydberg atoms in states $n \ll n_0$ originate from Penning ionization.

In an experiment similar to ours, van der Waal's attraction between very-high-*n* Rydberg atoms has been suggested as a mechanism for the enhancement of Rydberg-Rydberg collisions [18]. In our system, van der Waal's interactions are most likely insignificant in relation to the longer-range and stronger (permanent) electric-dipole interactions between high-*l* Rydberg atoms. Further, the mechanism we describe is more general and intrinsic to the dynamics of cold Rydberg gases than the previously observed electric-field-induced long-range *resonant* electric-dipole forces between Rydberg atoms [19]. In our system, interactions are nonresonant and forces are due to permanent electric-dipole moments. As a result, in our FI data the signatures of the Rydberg atoms in states $n \ll n_0$ are present whenever there is an appreciable amount of *l*-mixing signal (see Figs. 3 and 4).

D. Late arriving signal

When the FI pulse has reached its maximum value (at $\approx$220 V/cm), all Rydberg states down to $n \approx 40$ should be ionized (the exact limit depends on the parabolic quantum numbers). One expects there to be no signal after the FI pulse has reached its maximum. However, it is clear in Figs. 2–4 that a small signal is present even after the FI pulse has reached its maximum ("postmaximum FI signal"). More investigations will be required to determine the exact cause of the post-maximum FI signal. Presently, we believe that the postmaximum FI signal may be due to polar Rydberg atoms with ionization electric fields greater than the maximum of the FI pulse at the initial location of the atom cloud. Some of those polar Rydberg atoms may become pulled into regions of higher electric fields due to electric-dipole forces, as in an atomic-beam experiment described in [20]. As the atoms enter larger electric fields, they could ionize and give rise to the postmaximum FI signal.

VI. CONCLUSION

Upon some initial ionization, cold-Rydberg-atom gases easily develop a positive space charge that traps electrons for times on the order of tens of μs. The mechanism, which is analogous to one observed in cold plasmas [1], acts as a catalyst for electron-Rydberg atom collisions, increasing collision probabilities by orders of magnitude and profoundly altering the final state of the Rydberg gas. Using state-selective field ionization, we have provided direct proof for earlier claims that these collisions cause l mixing [4], and we have seen first experimental evidence that they also lead to inelastic n mixing, as predicted by theory [5]. We have found evidence for Rydberg-Rydberg collisions, enhanced by attractive electric-dipole forces between atoms in high-l states; these collisions apparently lead to Penning ionization and the appearance of Rydberg atoms in very-low-n Rydberg states. The degree to which the various collisional processes are observed depends on the initial Rydberg population, the initially excited Rydberg state, and the interaction time between the trapped electrons and the cold Rydberg gas.

The measurements described in this paper were performed in a vacuum system capable of cryogenic operation. Extending the measurements to a low-temperature environment (77 K and 4 K) will reduce blackbody radiation, allowing us to elucidate the role of blackbody radiation in cold Rydberg-gas and plasma dynamics. Low radiation temperatures will also dramatically increase the lifetime of the Rydberg atoms transferred into high-l states. Efforts are underway in our laboratory to trap Rydberg atoms in electrostatic, magnetostatic, and ponderomotive optical fields [21]. Long-lived high-l atoms generated in Rydberg gases and shielded in a cryogenic environment will be ideal subjects for this study. Another important perspective of the work on cold Rydberg gases and plasmas is its extension into the regime of strong magnetic fields. In this regime, strongly magnetized high-angular-momentum Rydberg atoms [22,23] may be generated and the preparation of strongly coupled two-component plasmas may be feasible.

ACKNOWLEDGMENTS

We wish to acknowledge fruitful discussions with Professor F. Robicheaux (Auburn University), Professor T. Gallagher (University of Virginia), and Professor E. Eyler (University of Connecticut). This work was supported by the National Science Foundation (Grant No. Phys-9875553). J.R.G. and J.-H.C. acknowledge support from the Chemical Sciences, Geosciences, and Biosciences Division of the Office of Basic Energy Sciences, Office of Science, U.S. Department of Energy.

[1] T. C. Killian, S. Kulin, S. D. Bergeson, L. A. Orozco, C. Orzel, and S. L. Rolston, Phys. Rev. Lett. **83**, 4776 (1999).
[2] M. P. Robinson, B. L. Tolra, M. W. Noel, T. F. Gallagher, and P. Pillet, Phys. Rev. Lett. **85**, 4466 (2000).
[3] T. C. Killian, M. J. Lim, S. Kulin, R. Dumke, S. D. Bergeson, and S. L. Rolston, Phys. Rev. Lett. **86**, 3759 (2001).
[4] S. K. Dutta, D. Feldbaum, A. Walz-Flannigan, J. R. Guest, and G. Raithel, Phys. Rev. Lett. **86**, 3993 (2001).
[5] F. Robicheaux and J. D. Hanson, Phys. Rev. Lett. **88**, 055002 (2002); F. Robicheaux and J. D. Hanson, Phys. Plasmas **10**, 2217 (2003).
[6] S. Mazevet, L. A. Collins, and J. D. Kress, Phys. Rev. Lett. **88**, 055001 (2002).
[7] S. G. Kuzmin and T. M. O'Neil, Phys. Rev. Lett. **88**, 065003 (2002).
[8] D. Feldbaum, N. V. Morrow, S. K. Dutta, and G. Raithel, Phys. Rev. Lett. **89**, 173004 (2002).
[9] T. F. Gallagher, *Rydberg Atoms* (Cambridge University Press, Cambridge, 1994), and references therein.
[10] Z. T. Lu, K. L. Corwin, M. J. Renn, M. H. Anderson, E. A. Cornell, and C. E. Wieman, Phys. Rev. Lett. **77**, 3331 (1996).
[11] R. J. Damburg and V. V. Kolosov, J. Phys. B **12**, 2637 (1979).
[12] C. Gabbanini, F. Ceccherini, S. Gozzini, and A. Lucchesini, J. Phys. B **31**, 4143 (1998).
[13] A. Walz-Flannigan, D. Feldbaum, S. K. Dutta, J. R. Guest, and G. Raithel, in *Proceedings of the Twenty-second International Conference on the Physics of Electronic and Atomic Collisions*, edited by J. Burgdoerfer, J. S. Cohen, S. Datz, and C. R. Vane (Rinton Press, Princeton, 2002).
[14] G. W. Foltz, E. J. Beiting, T. H. Jeys, K. A. Smith, F. B. Dunning, and R. F. Stebbings, Phys. Rev. A **25**, 187 (1982); R. G. Rolfes, D. B. Smith, and K. B. MacAdam, *ibid.* **37**, 2378 (1988).
[15] P. Mansbach and J. Keck, Phys. Rev. **181**, 275 (1969).
[16] C. E. Burkhardt, M. Ciocca, J. J. Leventhal, and J. D. Kelley, Phys. Rev. A **46**, 5795(1992).
[17] M. W. McGeoch, R. E. Schlier, and G. K. Chawla, Phys. Rev. Lett. **61**, 2088 (1988).
[18] E. Eyler (private communication).
[19] A. Fioretti, D. Comparat, C. Drag, T. F. Gallagher, and P. Pil-

let, Phys. Rev. Lett. **82**, 1839 (1999).
[20] G. Raithel, M. Fauth, and H. Walther, Phys. Rev. A **47**, 419 (1993).
[21] S. K. Dutta, J. R. Guest, D. Feldbaum, A. Walz-Flannigan, and G. Raithel, Phys. Rev. Lett. **85**, 5551 (2000).
[22] J. R. Guest, J.-H. Choi, and G. Raithel, Phys. Rev. A **68**, 022509 (2003).
[23] J. R. Guest and G. Raithel, Phys. Rev. A **68**, 052502 (2003).